Materials Chemistry and Physics 321 (2024) 129485

Contents lists available at ScienceDirect

Materials Chemistry and Physics

journal homepage: www.elsevier.com/locate/matchemphys

"Microwave approach and thermal decomposition: A sustainable way to produce ZnO nanoparticles with different chemo-physical properties"

Giovanna Gautier di Confiengo [a], Maria Giulia Faga [a], Valeria La Parola [b], Giuliana Magnacca [c], Maria Cristina Paganini [c], Maria Luisa Testa [b,*]

[a] CNR-STEMS, Strada Delle Cacce 73, 10135, Torino, Italy
[b] CNR-ISMN Istituto per Lo Studio Dei Materiali Nanostrutturati, Via Ugo La Malfa 153, 90146, Palermo, Italy
[c] Department of Chemistry and NIS Interdepartmental Centre, Torino University, Via Giuria 7, 10125, Torino, Italy

HIGHLIGHTS

- ZnO is easily produced by thermal decomposition (TD) and microwave-assisted (MW) procedures.
- MW method produces higher specific surface area samples, influencing nps size, with respect to TD approach.
- Melamine influence ZnO nps optical properties with the shift of band gap due to C3N4 formation.
- Sustainable ZnO synthesis is due to use of green chemicals, eco-friendly solvents and low-energy impact procedures.

GRAPHICAL ABSTRACT

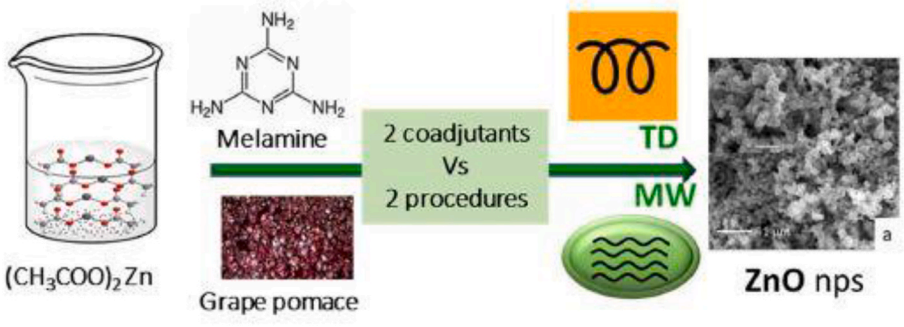

ARTICLE INFO

Keywords:
ZnO nps
MW-Assisted reaction
Thermal decomposition
C_3N_4
Band-gap

ABSTRACT

Two different synthetic approaches such as thermal decomposition method and microwave-assisted procedure were compared for the synthesis of nanosized ZnO. The two procedures were tested using zinc acetate as precursor as is, or in the presence of two coadjutants, one of anthropic origin (melamine) and one derived from the reuse of agricultural waste (wine extracts). All the samples were physico-chemically characterized in order to evaluate the influence of the synthesis conditions on the properties of the materials that were characterized by N_2 adsorption/desorption at 77 K and Field Emission-Scanning Electron microscopy measurements for evaluating the morphology, X-ray diffraction for examining the crystalline structure and X-Ray photoelectron spectroscopy for evidencing the surface composition of the nanoparticles. In order to verify the influence of the synthesis procedure on the electrical and optical properties of the ZnO nanoparticles, forecasting their use in photocatalytic applications, also the band gap of materials was evaluated by means of UV–Vis spectroscopy and Tauc plot. A final comparison of all the results allowed to evidence advantages and disadvantages of the procedures under study pointing out the importance of deepen the study of microwave-based synthetic approaches.

* Corresponding author.
E-mail address: marialuisa.testa@cnr.it (M.L. Testa).

https://doi.org/10.1016/j.matchemphys.2024.129485
Received 8 February 2024; Received in revised form 17 May 2024; Accepted 19 May 2024
Available online 24 May 2024

1. Introduction

Zinc oxide is a very interesting material since it can be very useful in a wide range of applications, such as cosmetics, effective sun protection, skin healing promoter, moisture adsorption, corrosion resistance and electronics. It is also suitable for low-cost solar cells, displays and sensors, but it is principally employed in semiconductors and diodes due to its electronic properties. It is well known for its wide band gap of 3.37 eV, large exciton binding energy of 60 meV at room temperature, and excellent chemical and thermal stability. The morphology and the physico-chemical properties of ZnO materials strictly depend on the synthetic strategies adopted for their preparation and literature reports several established techniques for the production of ZnO nanoparticles (nps).

ZnO nanopowder prepared through sol–gel route is described by Azam et al. [1] Zinc acetate dihydrate dissolved in ethylene glycol resulted in a highly water sensitive solution that easily converted into gel on addition of a few drops of water. The reaction carried out at 200 °C for 6h followed by the heating in two steps (450 °C for 8h and 700 °C for 5h) produces ZnO nanopowders. Standard precipitation method is widely used for the synthesis of ZnO nps [2]. From literature, several works reported this methodology as for in one-pot procedure [3] or by using a template free method [4] in free organic medium [5] or by basic aqueous precipitation at room temperature [6]. The described synthesis needed of several hours of reaction. Tsuchida et al. [7] reported the hydrolysis of zinc nitrate solution at 95 °C in presence of urea but the procedure yielded very small quantities of ZnO nps with a non-unique morphology (needles, rodsand spindles can be obtained). Solid-vapor sublimation technique [8] presents also some problems since it is quite sensitive to experimental conditions. One of the most used procedures is the hydrothermal method that usually occurs at temperature range of 80–100 °C consuming energy and a long time to reach crystallization temperature [9] allowing, at the same time, the control of size and shape of ZnO nps [10]. Despite the operating temperatures are not high, the process results inefficient in terms of energy transfer from source to reactants.

Due to problems related with high energy consumption, the emission of hazardous chemicals, the usage of complicated equipment, the industrial production of materials should be oriented, nowadays, toward sustainable synthetic procedures [11,12] which includes use of green chemicals and eco-friendly solvents and low-energy impact procedures.

For what concerns the use of green chemicals, in the last years a part of the research was focused on the use of natural extracts in the material synthesis [13]. The green chemistry approach to synthesizing nanoparticles uses plant extracts for metal ion reduction, with metabolites like sugars, terpenoids, polyphenols, alkaloids, phenolic acids, and proteins playing crucial roles. These compounds can act as reducing agents, lowering the valence state of metal ions, and replace toxic organic solvents with water or nontoxic alternatives [14], avoiding harmful chemicals and processes [15]. Venckatesh et al. used Aloe vera leaf extracts [16] were used in presence of zinc nitrate at 150 °C for 5–6 h, followed by a work-up reaction that included centrifugation, washing and drying (80 °C for 7–8 h) steps. According to the obtained results, it was found an effect of green extract on the morphology of ZnO nps achieving narrow particle size distribution around 35 nm. When Citrus peels extracts were used [17], the mixture was stirred at 80 °C for 10 min then calcined at 600 °C for 2h and the authors found higher crystallinity and larger particle size (of about 33 nm) of ZnO with respect to the commercial one. Another very recent study uses polyphenol extract from pepper waste [18]. The polyphenol extraction was carried out in presence of methanol and used to synthesize ZnO nps by colloidal precipitation. In this case $ZnCl_2$ was used as starting precursor, the mixture maintained at 50 °C for 2 h, filtered and calcined at 500 °C for 4 h giving smaller particles (24–43 nm) than those obtained with a classical precipitation method, without extract. Gur et al. obtained ZnO np of 6.5–7.5 nm with high antioxidant activity using zinc acetate dihydrate and Thymbra Spicata L [19]. Commelina Beghalensis was used in 2022 as a capping agent in the ZnO (NPs) production. Results showed that the nanoparticles had a hexagonal wurtzite structure and exhibit a variety of morphologies, including flaky platelets and spherical spheres [20]. %20 Spherical ZnO np of 32.8 nm of diameter was obtained using Garcinia Cambogia fruit pulp extract. The study confirms the good amphoteric and rapid activity of ZnOnp in photocatalytic dye degradation, demonstrating its ability to decompose both cationic and anionic organic dyes into harmless products [21]. Sedefoglu compared ZnO prepared with three different alkaline molar ratios (0.5 M, 1 M, and 2 M) and with and without calcination step. The study found that increasing NaOH molarity in a solution led to a decrease in the crystallite size of the final product. Moreover, significant enhancements in photocatalytic properties were observed after calcination, attributed to the changes in sample morphology from irregular shapes to spherical hexagonal forms and nanowires [22].

In order to study low-energy impact procedures, recently, microwave (MW) assisted methodologies are being applied to the synthesis of chemicals. This technology can be very useful in chemical processing because materials absorb the microwave irradiation instead of surface heating via convection and conduction as occurs in conventional reactions. The use of microwave irradiation allows rapid and uniform internal heating, leading to considerable energy and time saving and to a sustainable process. To the best of our knowledge, very few studies were published involving the use of MW-assisted synthesis of ZnO nps. The MW-assisted hydrothermal method [23] was applied for the synthesis of needle-shaped ZnO nps, irradiating zinc nitrate and urea in a Teflon bomb at 150W for 20 min. A long work-up of the reaction occurred, including 20h of cooling till room temperature and drying in oven 20h more. During the optimization procedure they found that no particles were produced if the irradiation occurred for less than 15 min at ca. 90 °C [24]. Mohammed et al. modified the procedure maintaining a zinc nitrate solution at 200 °C, irradiating at 1000W for 10 min [25]. The procedure occurred without template and no calcination step leading to stable ZnO nanorods employed for degrading dyes mixture and antibiotic pharmaceuticals. Single crystalline nanorods were synthetized by Rai et al. following a long procedure with a first step of 1 h needed for the precipitation of $Zn(OH)_2$ followed by the MW-assisted hydrothermal reaction in an autoclave at 150 °C for 1h more [26]. Recently, Aljaafari applied the MW-assisted hydrothermal method to produce ZnO nanosheets, through the precipitation of Zn acetate in basic medium, operating at 160 °C, 100psi, 1200W for 20 min [27].

In a view of an optimized and sustainable MW-assisted process, in this study we describe the synthesis of ZnO nps following a recent procedure that has been successfully demonstrated as being fast and effective in the preparation of materials [28,29]. Conventional thermal decomposition (TD) method was also carried out in order to study the influence of the synthetic approaches on the morphology and physico-chemical properties of ZnO nps. Taking into account the use of eco-compatible chemicals for the sustainability of the synthetic process, both methodologies were carried out by using Zn acetate as starting material, instead of the most used nitrate salt, avoiding toxic component release during the calcination step. Moreover, water was used as solvent and the effect of coadjutants, such as waste wine extracts (Barbera grape pomace) or melamine, on the physico-chemical properties of ZnO was also evaluated. Grape marc is a by-product of the wine industry, consisting of skins, seeds and stems. While the skins are rich in anthocyanins, the grape seeds are rich in extractable phenolic antioxidants such as phenolic acid, flavonoids, procyanidins and resveratrol, compounds that are essential for green synthesis [30].

In particular, by using different synthetic procedures, the use of melamine in presence of ZnO was recently studied by some of us, leading to the production of composites with interesting photocatalytic properties [31,32].

The textural, morphological/structural properties and surface composition of ZnO materials were investigated by means of N_2

adsorption isotherms, X-ray diffraction, Field Emission-Scanning Electron Microscopy and X-Ray photoelectron spectroscopy. Finally, in order to verify how the used synthetic approaches influence the electrical and optical properties of the ZnO nps, the evaluation of the band gap of materials was also carried out.

2. Materials and methods

All chemicals required for the synthesis of materials were used without any additional purification. Zinc acetate dihydrate, NH_4OH solution (28–30 %), melamine (99 %) were purchased by Aldrich. Grape pomace of Barbera extracts were prepared by CREA-VE (Italy) and used as they are [33,34].

2.1. Synthesis of ZnO nanoparticles

2.1.1. MW-assisted procedure (MW)

The following procedure was a modification of previous papers [28,29]. Zinc acetate dihydrate (9.5 g, 0.04 mol) was dissolved in deionized water (150 mL, 8.26 mol) then NH_4OH was added until pH 9. The mixture was treated with microwave (180W) during 20 cycles (20 s on, 10 s off corresponding to 6.40 min of irradiation). The white precipitate was filtered under vacuum, dried and calcined (in air, at 500 °C for 2h, 5 °C/min). The obtained powder is hereinafter labelled as ZnO/MW.

A similar procedure was carried out in the presence of grape pomace of Barbera extracts (E) or melamine (MEL). Extracts (E, 0.101 g) or Melamine (Mel, 4 g) were solubilized in deionized water (50 mL and 200 mL, respectively) and NH_4OH was added until pH 9. At the same time, zinc acetate dihydrate (6.41 g, 0.029 mol) solubilized in deionized water (50 mL) was added dropwise to the extract solution. The mixture was treated with microwaves (180W) during 20 cycles (20 s on, 10 s off for a total irradiation time of 6.40 min). The white precipitate was filtered under vacuum, dried (90 °C, overnight) and then calcined (in air, at 500 °C for 2h, 5 °C/min). The material is hereinafter labelled as ZnO/E/MW and ZnO/MEL/MW respectively.

2.1.2. Thermal decomposition method (TD)

The thermal decomposition synthesis procedure was developed on basis of previous works [35]. Extracts (E) or melamine (Mel) (0.105 g) were dissolved in 120 ml of water at room temperature and stirred at room temperature for 2 h. After that 6.42 g of zinc acetate dihydrate was added and stirred for 1 h. The solutions were then dried at 90 °C to form a paste and then calcined in a muffle furnace (in air, at 500 °C for 2h, 5 °C/min). The materials are hereinafter labelled as ZnO/E/TD and ZnO/MEL/TD, respectively. For comparison purpose, ZnO without any coadjutants was produced following the same procedure and the material is hereinafter labelled as ZnO/TD.

2.2. Characterization of ZnO particles

The textural properties were obtained by N_2 adsorption/desorption isotherms using Micromeritics ASAP2020 Plus 1.03 (Micromeritics, Norcross, GA 30093, USA). Before the analyses, samples were outgassed at 100 °C for 4 h to clean the surface and make also the pores available for N2 adsorption. The fully computerized analysis of the N_2 adsorption isotherm at −196 °C in the standard pressure range 0.05–0.3 p/p0 allowed us to obtain, through Brunauer–Emmett–Teller (BET) model, the specific surface areas (SSA) of the samples. The micropore presence was evaluated using the t-plot method. The total pore volume (Vp) and pore size distribution (dV/dw)) were evaluated by applying the Barrett–Joyner–Halenda (BJH) model to the desorption branch of isotherms.

The crystal structure of ZnO nanoparticles were examined using powder X-ray diffraction (XRD). XRD patterns were recorded by X-ray diffractometer Malvern Panalytical X'Pert Pro (Malvern, UK) equipped with an X'Celerator detector using Cu Kα radiation generated at 45 kV and 40 mA within a 2θ range of 20°–80°. The JCPDS Card No. 36–1451, which contains standards produced by the Joint Committee on Powder Diffraction and Standards (JCPDS), was used to compare the patterns. The crystallite size and lattice strain of ZnO were calculated from the broadening of the XRD peaks using Williamson–Hall approach, according to equation (1):

$$\beta \cos\theta = \frac{k\lambda}{D} + 4\varepsilon \sin\theta \qquad \text{eq (1)}$$

where k is the shape factor, λ is the wavelength of incident X-ray, β is the Full Width at Half Maximum (FWHM) measured in radians and θ is the Bragg angle of diffraction peak. The term "βcosθ" was plotted against "4sinθ" for all orientation peaks of ZnO varying from 20° to 80°, in order to perform a Williamson-Hall analysis. Crystallite size and strain are calculated from the slope and y-intercept of a straight line that is fitted to the data.

Field emission scanning electron microscopy (FESEM TESCAN S9000G, Brno, Czech Republic) was used to analyze the particles' size and shape. Samples were coated with a Cr coating 5 nm thick prior to FESEM analysis. Using the ImageJ program, the mean ZnO np diameters were calculated from FESEM images. Being no perfectly spherical particles, the longest dimension was reported for highlighting the main differences among the samples.

X-ray photoelectron spectroscopy analysis was performed with a VGMicrotech ESCA 3000 Multilab (VG Scientific, Sussex, UK), equipped with a dual Mg/Al anode. The spectra were excited by the unmonochromatized MgK α source (1253.6 eV) run at 14 kV and 15 mA. The analyzer operated in constant analyzer energy (CAE) mode. For the individual peak energy regions, a pass energy of 20 eV set across the hemispheres was used. Survey spectra were measured at 50 eV pass energy. The sample powders were analyzed as powder mounted on a double-sided adhesive tape. The pressure in the analysis chamber was of the order of 10-8 Torr during data collection. The invariance of the peak shapes and widths at the beginning and end of the analyses ensured the absence of differential charging. Analyses of the peaks were performed with the Casa XPS software Version 2.3.18PR1.0. Atomic concentrations were calculated from peak intensity using the sensitivity factors provided with the software. The binding energy values are quoted with a precision of ±0.15 eV and the atomic percentage with a precision of ±10 %.

Diffuse Reflectance (DR) UV–vis spectroscopy was used to perform an optical characterization of the semiconductor samples and determine their band gap. The optical spectra were recorded utilizing a Varian Cary 5000 spectrophotometer from Agilent (CA, USA), and the data were processed with the Carywin-UV/scan software, also from Agilent (CA, USA). As a reference, we used a sample of PTFE with 100 % reflectance. Subsequently, the optical band gap energies were determined through the application of the Tauc plot method to the collected spectra. It's important to note that the magnitude of the energy gap is directly related to the absorption coefficient near the absorption edge and is contingent upon the specific type of transition (whether direct or indirectly allowed) [36].

3. Results and discussion

The textural properties obtained by N_2 gas-volumetric adsorptions show, in all cases, isotherms of the IV type, typical of mesoporous systems.

The main results of the investigation are reported in Table 1, as specific surface area and total mesopore volume. The specific surface areas of the samples are quite limited, but the MW-assisted synthesis shows higher areas and higher mesopore volumes with respect to TD method. The t-plot (not reported for the sake of brevity) allows excluding the presence of micropores, whereas BJH model gives the pore size distribution reported in Fig. 1, bottom section. The curves suggest

Table 1
Textural properties of the samples.

Sample	BET surface area (m^2/g) ± model uncertainty	Vp (cm^3/g)
ZnO/MW	14.2 ± 0.7	0.08
ZnO/Mel/MW	21.0 ± 1.0	0.07
ZnO/E/MW	18.4 ± 0.9	0.11
ZnO/TD	7.5 ± 0.3	0.04
ZnO/Mel/TD	7.4 ± 0.3	0.04
ZnO/E/TD	7.4 ± 0.3	0.04

that TD synthesis is not sensitive to the presence of different coadjutants, as all samples show essentially only mesopores smaller than 10 nm of width. Otherwise, the coadjutant used affects the MW-assisted synthesis, as the presence of the small melamine molecules promotes the formation of small mesopores of about 10 nm of width, whereas larger extract matrices produce larger mesopores of about 100 nm of width In addition, TD method produces materials with a more limited mesopore volume, i.e., denser with respect to MW one, as indicated by the data in the third column of Table 1.

Fig. 2 depicts the ZnO powders XRD pattern. The diffraction peaks related to the (hkl) planes were observed: (100), (002), (101), (102), (110), (103), (200), (112), (201) and (202) attributable to the formation of wurtzite-type ZnO particles with a hexagonal structure [37]. For all samples, the peak corresponding to (101) is the most intense and it was used to normalize the X-ray diffraction patterns. The relative intensity of the peaks 100, 002 and 101 is almost similar for all the samples. Table 2 shows the relative intensity values with respect to the peak 002 (c-axis orientation) and the value is approximately 0.25 for all samples. It can be seen that ZnO prepared by microwave always shows a higher value than that prepared by thermal synthesis, probably as a result of variations in thermal development leading to variable crystallite formation [38]. The absence of additional diffraction peaks of Zn, $Zn(OH)_2$, or other ZnO phases suggests that the proposed methods result in pure ZnO crystalline nps. The high purity and the good crystallinity of the sample are confirmed by the sharp, narrow peak intensity. The structural parameters of the ZnO nanoparticles were determined including their *a* and *c* lattice parameters and the unit cell volume (V) using the following formula:

$$a = \frac{\lambda}{\sqrt{3}\ \sin\theta} \quad \text{eq(2)}$$

$$c = \frac{\lambda}{\sin\theta} \quad \text{eq(3)}$$

$$V = \frac{\sqrt{3}}{2} a^2 c \quad \text{eq(4)}$$

The volume V and lattice parameters c and a of the ZnO nps synthesized in this study, shown in Table 2, are compared with the values found in JCPDS file no. 36–1451, together to crystallite size and strain calculated using Williamson-Hall (W–H) which graphs are not reported

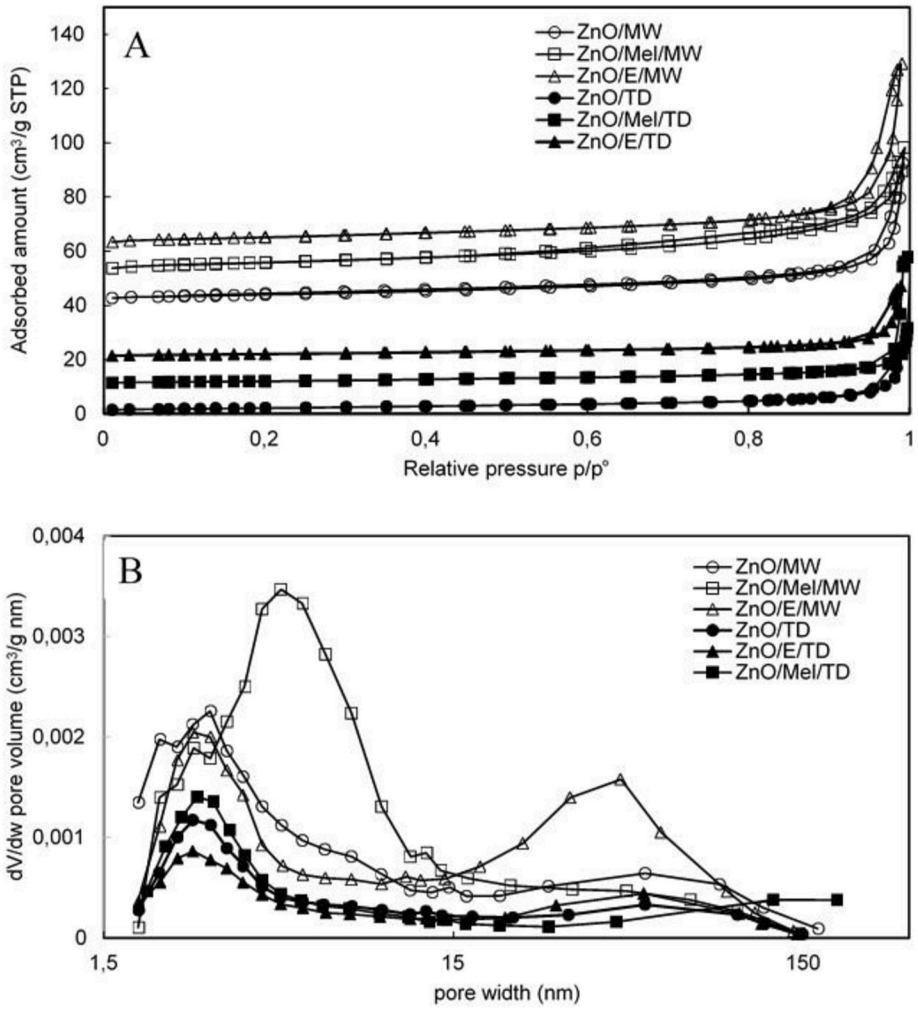

Fig. 1. Section A: adsorption/desorption isotherms of N_2 adsorbed at −196 °C (the curves have been shifted for the sake of clarity); Section B: pore size distribution from BJH model (desorption branch).

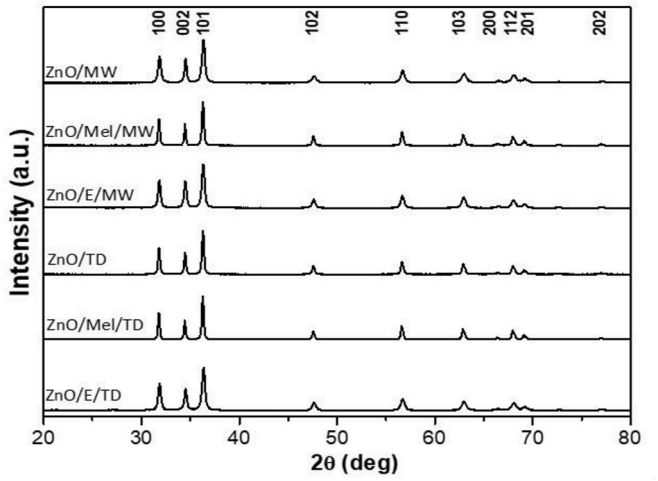

Fig. 2. XRD patterns of ZnO.

Table 2
Structural parameters of ZnO.

Samples	D_S (nm)[i]	I(002)/[I(100) + I(002) + I(101)][ii]	a[iii]	c[iii]	V[iv]	D_{W-H} (nm)[v]	Strain 10^{-3} [vi]
ZnO/MW	138 ± 17	0.259	3.2434	5.2734	48.04	43.91	2.7
ZnO/Mel/MW	104 ± 18	0.237	3.2491	5.1968	47.50	37.16	2.2
ZnO/E/MW	73 ± 18	0.274	3.2460	5.2777	48.15	45.29	2.3
ZnO/TD	125 ± 36	0.234	3.2489	5.2819	48.29	69.01	1.7
ZnO/Mel/TD	149 ± 71	0.212	3.2503	5.2075	47.64	69.01	1.5
ZnO/E/TD	157 ± 30	0.241	3.248	5.2812	48.26	90.58	2.2
JCPDS Card No. 36-1451[vii]			3.2498	5.2066	47.62		

i) Average particle size of the sintered ZnO measured by ImageJ software from FESEM images; ii) Relative intensities of (0 0 2) peaks of ZnO particles; iii) Lattice constants a,c, iv) Volume, v) Crystallite size; vi) Lattice strain calculated by Williams-Hall methodology, vii) The XRD values of ZnO reference card 36–1451 are indicated for comparison.

for the sake of brevity.

The obtained values resulted very close to the tabulated ones, in particular, those prepared in presence of melamine. With regard to crystallite size, by using the Williamson Hall method the analysis confirms that nanoparticles produced with microwave synthetic approach present a smaller size than those obtained with thermal decomposition method.

Fig. 3 shows FESEM images at different magnification of ZnO. Nanoparticles are mostly spherical/oval in shape, with a smooth surface. A tendency towards aggregation into irregular structures can be observed under all conditions. This is most evident for ZnO synthesized using extracts, where aggregates result more compact. Table 2 reports the findings of the calculation of the average particle size (Ds) using at least 50 particles. No difference between thermal process and microwave treatment can be observed on the particles diameter when any coadjutant is used for the synthesis of ZnO nps (Fig. 3a and d and Table 2). When extract or melamine are used, microwave process results in a reduction of the particles diameter with respect to the thermal process. This phenomenon is particularly relevant in the presence of extract, for which diameter is halved (73 nm).

In order to analyze the surface of ZnO materials synthesized by the two different methods XPS analysis was performed. Zn 2p lines are not very sensible to chemical environments and Zn 2p3/2 at 1021.7 eV has been used to compensate the charging problems [39]. The evaluation of the chemical state has been done by means of the analysis of the Auger Zn $L_3M_{4,5}M_{4,5}$ and α' parameters (reported in Table 3). All the α' parameters are in the range indicated for ZnO [40]. A lower α' parameter is shown by ZnO synthesized using the extract indicating a decrease of valence electron density on Zn [41] probably due to the interaction with the extract. The sample prepared by microwave procedure with melamine shows the presence of a peak at 399.8 eV due to the residual nitrogen and a peak at 288.7 eV (outlined by an arrow in the inset of Fig. 4) in the carbon region. These features are compatible with the formation of carbon nitride [42]. Interestingly, sample ZnO/Mel/TD does not favor the formation of carbon nitride and, after calcination, no residual nitrogen is present.

The deconvolution of the O1s region, shown in Fig. 5 and in Table 3 and is typical of a ZnO oxide. The peak can be deconvoluted in two main components at 530.2 eV attributed to oxygen by the lattice and a component at higher binding energy (ca. 532eV) attributed to terminal hydroxyl groups on the surface of the oxide. The distribution of these two components is the same for all samples, except for ZnO/Mel/MW where the absence of the hydroxyl component due to the formation of carbon nitride is observed.

Finally, the values of the materials band gap were evaluated to understand how the two different synthetic approaches influence the electronic properties of the ZnO nps. As described in Fig. 6, all the ZnO materials exhibit very similar behaviors. The calculation of the energy gap values via the Tauc plot method was performed; all the data are presented in Table 3. The values of the band gap for all materials are very similar and close to that of pure ZnO material. The increased absorption of visible light (and consequently the lower percentage of reflectance) in the case of the samples produced by TD method, can be ascribed to the presence of carbon, evident by the grey color of the material due to the thermal decomposition of Zinc acetate. With this procedure it is common to trap some carbon residual particles inside the structure, the oxidation process cannot avoid the formation of these clusters and the result is a grey sample (spectra d, e, f). The materials prepared by the microwave-assisted procedure show a higher percentage of reflectance, in particular the sample of pure ZnO (spectrum a), sample obtained by the coupling of ZnO with melamine (spectrum b) presents a deep absorption shoulder in the region of the visible light with a maximun in the absorption at around 530 nm, in fact the sample presents a pale-yellow color. Besides the presence of unavoidable intrinsic defects, this deep absorption shoulder could be due to the formation of carbon nitride (C_3N_4) obtained by the decomposition of melamine at high temperature, whose presence is also confirmed by XPS analysis. This behavior has been already observed and described elsewhere by some of us [31,32]. The presence of carbon nitride allows the formation of C_3N_4–ZnO composite that can improve the photocatalytic properties making possible the absorption of visible light. With respect to the previous study [32], although maintaining the same band-gap, the microwaves allow a rapid and efficient procedure. The sample obtained with ZnO and grape pomace of Barbera extracts causes the decrease in the percentage of absorbance and the modification of the sample color. The two preparation methods lead to the formation of different samples even if the band gap is not affected by the procedures. It seems also that the presence of both coadjutants (grape pomace and melamine) in both the preparation approaches, leads to the change in the color of sample allowing a possible absorption activity in the visible light range. In the meantime, the Urbach energy (Eu) was calculated by assessing the breadth of the energy bands' tails caused by localized states within the forbidden band. This parameter is thought to be associated with the

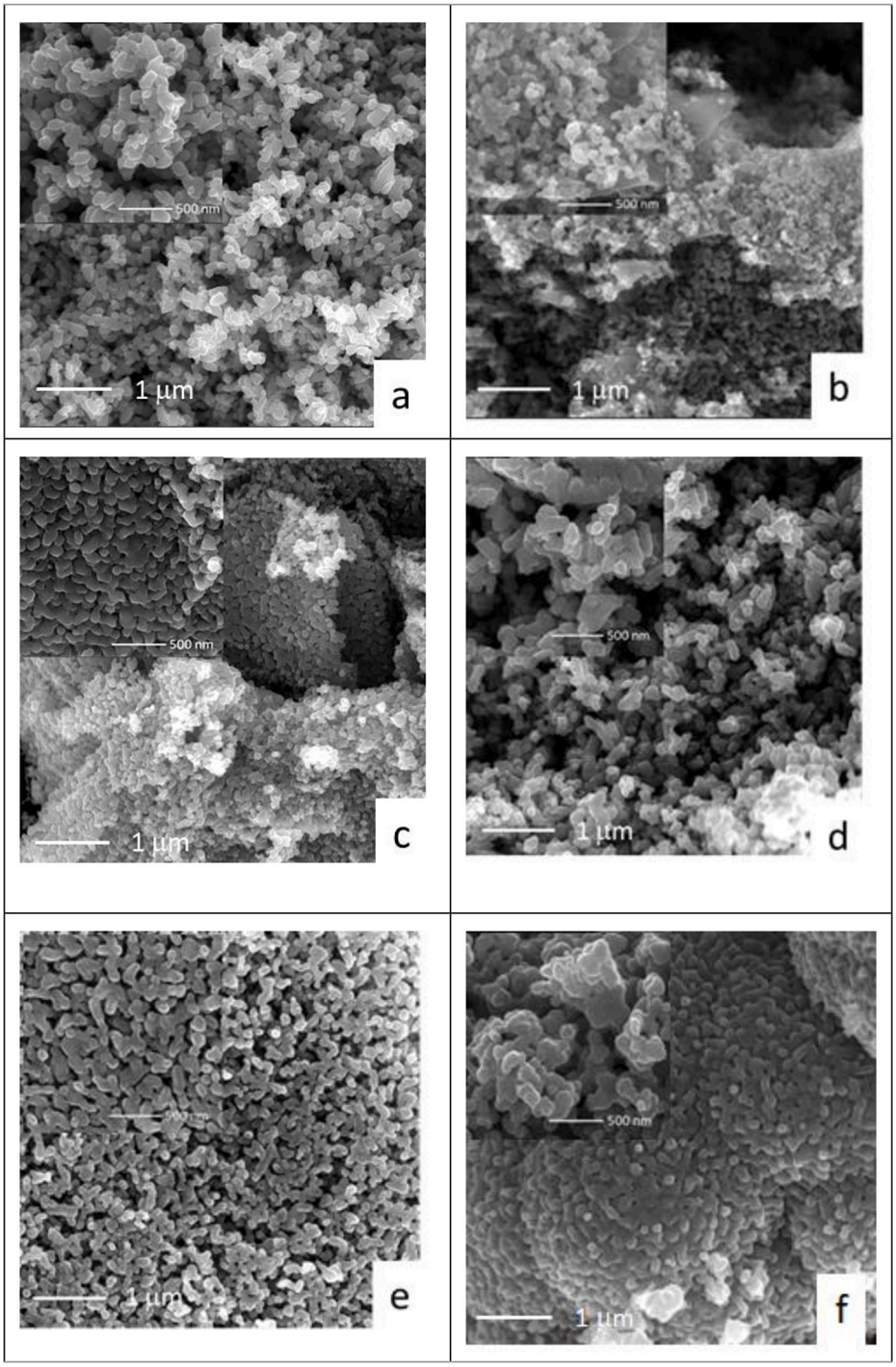

Fig. 3. FESEM micrographic image of a) ZnO/MW, b) ZnO/Mel/MW, c) ZnO/E/MW, d) ZnO/TD, e) ZnO/Mel/TD f) ZnO/E/TD.

Table 3
O1s binding energy (eV), α' values calculated by XPS Zn 2p3/2-$L_3M_{45}M_{45}$ Auger peaks and Band Gap values from Tauc plot, and Urbach Energy.

Sample	O1s (eV)	α′	BG (eV)	Eu (meV)
ZnO/MW	530.2 (57 %) 531.8 (43 %)	2010.9	3.23	93
ZnO/Mel/MW	530.6 (100 %)	2009.5	3.19	146
ZnO/E/MW	530.5 (61 %) 532.1 (39 %)	2008.7	3.20	107
ZnO/TD	530.1 (60 %) 531.7 (40 %)	2009.7	3.12	155
ZnO/Mel/TD	529.7 (61 %) 531.7 (39 %)	2009.0	3.22	177
ZnO/E/TD	529.5 (65 %) 531.4 (35 %)	2009.2	3.18	135

structural irregularities present in the material. The values for the Urbach Energy have been reported in Table 3. The absorption coefficient of the material shows a tail corresponding to the so-called Urbach tail, for sub-band gap photon energy. It is closely related to the disorder in the crystalline lattice and is expressed as $\alpha = \alpha 0 \exp(h\nu/Eu)$ with α0 a constant, Eu the Urbach energy is directly involved in the slope of the exponential edge [43]. The above equation describes the optical transition between occupied states in the valence band tail to unoccupied states of the conduction band edge. Fig. 6 shows %R as a function of wavelength (nm). The value of Eu was obtained from the inverse of the slope of ln(α) versus (hν). A lower value of Urbach Energy corresponds to a lower concentration of defects in the crystalline material. According to

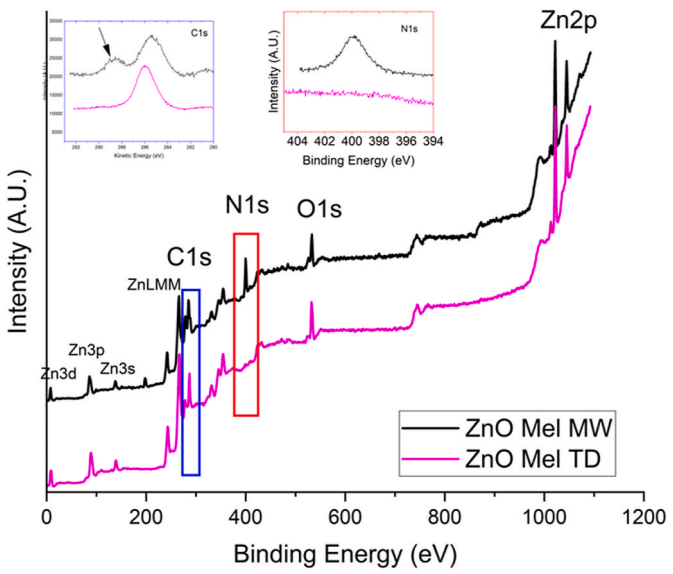

Fig. 4. XPS Survey spectra of ZnO/Mel/MW and ZnO/Mel/TD. The C1s and N1s regions are shown in the blue and red inset respectively. (For interpretation of the references to color in this figure legend, the reader is referred to the Web version of this article.)

the values reported in Table 3 pure ZnO presents the lower value of Eu while the formation of composites lead to the increase of Eu and so to defects in the structure. High numbers of Urbach energy for the samples obtained via Thermal Decomposition (TD) are due to the presence of residual carbon particles, derived from acetate decomposition, trapped in the crystalline systems.

4. Conclusion

With the focus to make more sustainable the synthetic procedures of materials in terms of use of green chemicals, eco-friendly solvents and low-energy impact procedures, this study compares two different methodologies for the production of ZnO nanoparticles, namely the classical TD method and the more innovative MW-assisted one, with and without coadjutants such as waste wine extract and melamine. MW-assisted procedure showed different advantages with respect to TD one. In fact, it resulted very efficient in terms of reaction time: just 6.40

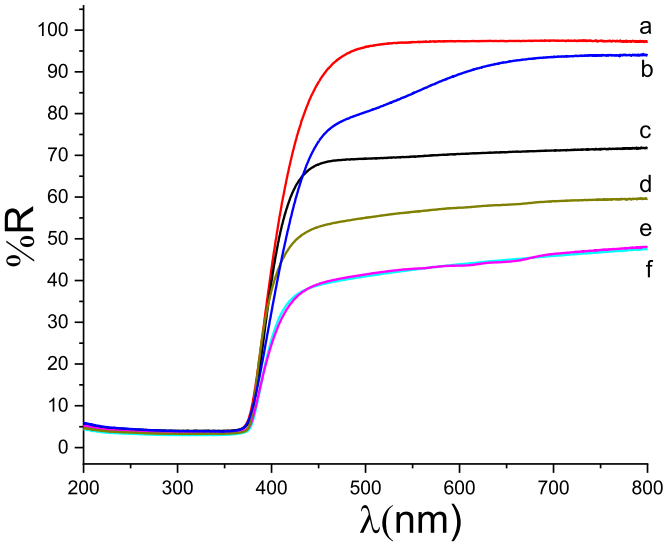

Fig. 6. DR-UV VIS spectra of a) ZnO/MW, b) ZnO/Mel/MW, c) ZnO/E/MW, d) ZnO/TD, e) ZnO/Mel/TD, f) ZnO/E/TD.

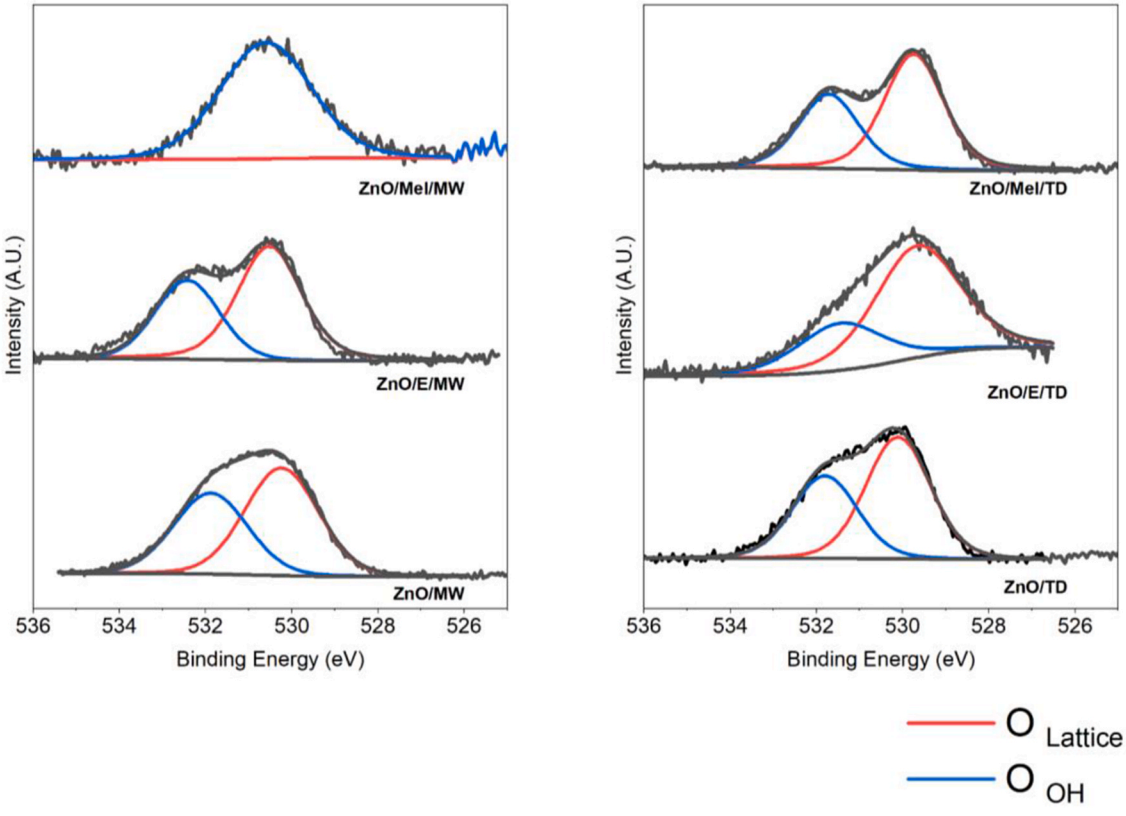

Fig. 5. XPS O1s region of ZnO samples prepared by different methods.

min of irradiation at 180W allowed the formation of ZnO nps with a twofold surface area and pore volume with respect to that produced by TD method. The effect is even more evident in the presence of both extracts and melamine. XRD and FESEM analysis confirm that microwave influences the size of nanoparticles which results in the range of 37–45 nm regardless of coadjuvant presence, whereas crystallite size of 90 nm is observed applying the TD method in the presence of extract. The MW approach also affects the reaction products, as XPS and UV–Vis spectroscopy reveal the presence of C_3N_4 formed by melamine decomposition, which causes the variation of ZnO band gap (and probably also an improvement of its photocatalytic activity) for the sample ZnO/Mel/MW.

In conclusion, the use of MW-assisted method seems advantageous with respect to the classical TD approach, as it produces higher specific surface area samples for which the interaction with substrates (pollutants, for instance) should be enhanced. The presence of coadjutants improves the dispersion and probably the reactivity of ZnO nps, as the specific surface area increases (being slightly better in the presence of melamine), but it does not change the band gap which remains at 3.20 eV. In addition, melamine seems very interesting for the optical properties of the synthesized ZnO nps, given the production of carbon nitride. Further studies are needed to investigate the actual photocatalytic activity of these materials and the real advantage brought by melamine use in terms of sustainability of the process.

CRediT authorship contribution statement

Giovanna Gautier di Confiengo: Writing – original draft, Investigation, Formal analysis. **Maria Giulia Faga:** Writing – original draft, Data curation. **Valeria La Parola:** Writing – original draft, Investigation, Data curation. **Giuliana Magnacca:** Writing – review & editing, Writing – original draft, Investigation, Data curation. **Maria Cristina Paganini:** Writing – original draft, Investigation, Data curation. **Maria Luisa Testa:** Writing – review & editing, Writing – original draft, Supervision, Investigation, Data curation, Conceptualization.

Declaration of competing interest

The authors declare that they have no known competing financial interests or personal relationships that could have appeared to influence the work reported in this paper.

Data availability

No data was used for the research described in the article.

Acknowledgments

CREA -VE is acknowledged for the furniture of grape pomace Barbera extracts.

References

[1] A. Azam, F. Ahmed, N. Arshi, M. Chaman, A.H. Naqvi, Formation and characterization of ZnO nanopowder synthesized by sol–gel method, J. Alloys Compd. 496 (2010) 399–402, https://doi.org/10.1016/j.jallcom.2010.02.028.
[2] Y. Xia, J. Wang, R. Chen, D. Zhou, L. Xiang, A review on the fabrication of hierarchical ZnO nanostructures for photocatalysis application, Crystals 6 (2016) 148–167, https://doi.org/10.3390/cryst6110148.
[3] B. Reeja-Jayan, E. de la Rosa, A. Torres-Castro, V. Gonzalez-Gonzalez, M. J. Yacaman, S. Sepulveda-Guzman, Synthesis of assembled ZnO structures by precipitation method in aqueous media, Mater. Chem. Phys. 115 (2009) 172–178, https://doi.org/10.1016/j.matchemphys.2008.11.030.
[4] J. Wang, L. Gao, Synthesis and characterization of ZnO nanoparticles assembled in one-dimensional order, Inorganic Chemistry Commun 6 (2003) 877–881, https://doi.org/10.1016/S1387-7003(03)00134-5.
[5] L. Laânab, B. Jaber, One step synthesis of ZnO nanoparticles in free organic medium: structural and optical characterizations, Mater. Sci. Semicond. Proces. 27 (2014) 446–451, https://doi.org/10.1016/j.mssp.2014.07.025.
[6] K.P. Raj, K. Sadayandi, Effect of temperature on structural, optical and photoluminescence studies on ZnO nanoparticles synthesized by the standard co-precipitation method, Physica B 487 (2016) 1–7, https://doi.org/10.1016/j.physb.2016.01.020.
[7] T. Tsuchida, S. Kitajima, Preparation of uniform zinc oxide particles by homogeneous precipitation from zinc sulfate and nitrate solutions, Chem. Lett. (1990) 1769, https://doi.org/10.1246/cl.1990.1769.
[8] S. Kar, A. Dev, S. Chaudhuri, Simple solvothermal route to synthesize ZnO nanosheets, nanonails, and well-aligned nanorod arrays, J. Phys. Chem. B 110 (2006) 17848–17853, https://doi.org/10.1021/jp0629902.
[9] H. Hayashi, Y. Hakuta, Hydrothermal synthesis of metal oxide nanoparticles in supercritical water, Materials 3 (2010) 3794–3817, https://doi.org/10.3390/ma3073794.
[10] B. Cheng, E.T. Samulski, Hydrothermal synthesis of one-dimensional ZnO nanostructures with different aspect ratios, Chem. Commun. (2004) 986–987, https://doi.org/10.1039/B316435G.
[11] A. Rana, K. Yadav, S. Jagadevan, A comprehensive review on green synthesis of nature-inspired metal nanoparticles: mechanism, application and toxicity, J. Cleaner Prod. (2020) 122880–122905, https://doi.org/10.1016/j.jclepro.2020.122880.
[12] C.J. Li, B.M. Trost, Green chemistry for chemical synthesis, Proc. Natl. Acad. Sci. USA 105 (2008) 13197–13202, https://doi.org/10.1073/pnas.0804348105.
[13] K. Parveen, V. Banse, L. Ledwani, Green synthesis of nanoparticles: their advantages and disadvantages, AIP Conf. Proc. 1724 (2016) 020048, https://doi.org/10.1063/1.4945168.
[14] C.J. Li, Reflection and perspective on green chemistry development for chemical synthesis Green, Chem 18 (2016) 1836, https://doi.org/10.1039/c6gc90029A.
[15] R.A. Sheldon Green solvents for sustainable organic synthesis: state of the art, Green Chem. 7 (2005) 267–278, https://doi.org/10.1039/B418069K.
[16] G. Sangeetha, S. Rajeshwari, R. Venckatesh, Green synthesis of zinc oxide nanoparticles by aloe barbadensis miller leaf extract: structure and optical properties, Mater. Research Bull 46 (2011) 2560–2566, https://doi.org/10.1016/j.materresbull.2011.07.046.
[17] Y. Gao, D. Xu, D. Ren, K. Zeng, X. Wu, Green synthesis of zinc oxide nanoparticles using Citrus sinensis peel extract and application to strawberry preservation: a comparison study, LWT 126 (2020) 109297–109305, https://doi.org/10.1016/j.lwt.2020.109297.
[18] M. Jiménez-Rosado, A. Gomez-Zavaglia, A. Guerrero, Romero Green synthesis of ZnO nanoparticles using polyphenol extracts from pepper waste (Capsicum annuum), J. Cleaner Prod. 350 (2022) 131541–131552, https://doi.org/10.1016/j.jclepro.2022.131541.
[19] G. Tugba, I. Meydan, H. Seckin, M. Bekmezci, F. Sen, Green synthesis, characterization and bioactivity of biogenic zinc oxide nanoparticles, Environ. Res. 204 (2022) 111897–111904, https://doi.org/10.1016/j.envres.2021.111897.
[20] D.A. Bopape, D.E. Motaung, N.C. Hintsho-Mbita, Green synthesis of ZnO: effect of plant concentration on the morphology, optical properties and photodegradation of dyes and antibiotics in wastewater, Optik 251 (2022) 168459–168476, https://doi.org/10.1016/j.ijleo.2021.168459.
[21] S. Sasi, P.H.F. Fasna, T.K.B. Sharmila, C.S.J. Chandra, J.V. Antony, V. Raman, A. B. Nair, H.N. Ramanathan, Green synthesis of ZnO nanoparticles with enhanced photocatalytic and antibacterial activity, J. Alloy Com 924 (2022) 166431–166446, https://doi.org/10.1016/j.jallcom.2022.166431.
[22] N. Sedefoglu, Characterization and photocatalytic activity of ZnO nanoparticles by green synthesis method, Optik 288 (2023) 171217–171228, https://doi.org/10.1016/j.ijleo.2023.171217.
[23] D. Ledwith, S.C. Pillai, G.W. Watson, J.M. Kelly, Microwave induced preparation of a-axis oriented double-ended needle-shaped ZnO microparticles, Chem. Commun. (2004) 2294–2295, https://doi.org/10.1039/B407768G.
[24] S.C. Padmanabhan, D. Ledwith, S.C. Pillai, D.E. McCormack, J.M. Kelly, Microwave-assisted synthesis of ZnO micro-javelins, J. Mater. Chem. 19 (2009) 9250–9259, https://doi.org/10.1039/B912537J.
[25] R. Mohammed, M.E.M. Ali, E. Gomaa, M. Mohsen, Highly stable, reusable, and MW-assisted prepared ZnO nanorods for wastewater decontamination: precursors ratios effect and insights on matrix and pollutants mineralization, J. Environ. Chem. Eng. 9 (2021) 104630–104645, https://doi.org/10.1016/j.jece.2020.104630.
[26] P. Rai, H.M. Song, Y.S. Kim, M.-K. Song, P.R. Oh, J.M. Yoon, Y.T. Yu, Microwave assisted hydrothermal synthesis of single crystalline ZnO nanorods for gas sensor application, Mater. Lett. 68 (2012) 90–93, https://doi.org/10.1016/j.matlet.2011.10.029.
[27] A Aljaafari size dependent photocatalytic activity of ZnO nanosheets for degradation of methyl red, Front. Mater. 7 (2020) 562693–562700, https://doi.org/10.3389/fmats.2020.562693.
[28] A. Emamdoust, V. La Parola, G. Pantaleo, M.L. Testa, S. Farjami Shayesteh, A. M. Venezia, Partial oxidation of methane over SiO2 supported Ni and NiCe Catalysts, J. Energy Chemistry 47 (2020) 1–9, https://doi.org/10.1016/j.jechem.2019.11.019.
[29] M. Russo, V. La Parola, G. Pantaleo, M.L. Testa, A.M. Venezia, R. GuptaA Bordoloi, R. Bal, Structural insight in TiO_2 supported CoFe catalysts for Fischer -Tropsch synthesis at ambient pressure, Appl. Catal. Gen. 600 (2020) 117621–117629, https://doi.org/10.1016/j.apcata.2020.117621.
[30] J. Yu, M. Ahmedna, Functional components of grape pomace: their composition, biological properties and potential applications, Int J. Food Science Techn. 48 (2013) 221–237, https://doi.org/10.1111/j.1365-2621.2012.03197.x.

[31] E. Cerrato, M.C. Paganini, Mechanism of visible photon absorption: unveiling of the C3N4-ZnO photoactive interface by means of EPR spectroscopy, Mater. Adv. 1 (2020) 2357–2367, https://doi.org/10.1039/d0ma00451k.
[32] A. Actis, F. Sacchi, C. Takidis, M.C. Paganini, E. Cerrato, Changes in structural, morphological and optical features of differently synthetized C3N4-ZnO heterostructures: an experimental approach, Inorganics 10 (2022) 119–133, https://doi.org/10.3390/inorganics10080119.
[33] M. Guaita, L. Panero, S. Motta, B. Mangione, A. Bosso, Effects of high-temperature drying on the polyphenolic composition of skins and seeds from red grape pomace, LWT 145 (2021) 111323, https://doi.org/10.1016/j.lwt.2021.111323.
[34] M. Guaita, S. Motta, S. Messina, F. Casini, A. Bosso, Polyphenolic profile and antioxidant activity of green extracts from grape pomace skins and seeds of Italian cultivars, Foods 12 (2023) 3880, https://doi.org/10.3390/foods12203880.
[35] F. Adam, A. Himawan, M. Aswad, S. Ilyas, M. Heryanto, A. Anugrah, D. Tahir, Green synthesis of zinc oxide nanoparticles using Moringa oleifera l. water extract and its photocatalytic evaluation, J. J. Phys.: Conf. Ser. 1763 (2021) 012002, https://doi.org/10.1088/1742-6596/1763/1/012002.
[36] J. Tauc, The Optical Properties of Solids, Academic Press, New York, 1966.
[37] T. Harma, M. Garg, Optical and morphological characterization of ZnO nano-sized powder synthesized using single step sol-gel technique, Opt. Mater. 132 (2022) 112794–112802, https://doi.org/10.1016/j.optmat.2022.112794.
[38] C. Jaramillo-Paez, P. Sánchez-Cid, J.A. Navío, M.C. Hidalgo, A comparative assessment of the UV-photocatalytic activities of ZnO synthesized by different routes, J. Environ. Chem. Engineering (2018) 7161–7171, https://doi.org/10.1016/j.jece.2018.11.004.
[39] C. Woll, The chemistry and physics of zinc oxide surfaces, Prog. Surf. Sci. 82 (2007) 55–120, https://doi.org/10.1016/j.progsurf.2006.12.002.
[40] L. Dake, D. Baer, J. Zachara, Auger parameter measurements of zinc compounds relevant to zinc transport in the environment, Surf. Interface Analysis 14 (1989) 71–75, https://doi.org/10.1002/sia.740140115.
[41] M. Futsuhara, K. Yoshioka, O. Takai Structural, Electrical and optical properties of zinc nitride thin films prepared by reactive rf magnetron sputtering, Thin Solid Films 322 (1998) 274–281, https://doi.org/10.1016/S0040-6090(97)00910-3.
[42] X. Li, J. Zhang, L. Shen, Y. Ma, W. Lei, Q. Cui, G. Zou, Preparation and characterization of graphitic carbon nitride through pyrolysis of melamine of carbon nitride, Appl Phys A 94 (2009) 387–392, https://doi.org/10.1007/s00339-008-4816-4.
[43] K. Boubaker, A physical explanation to the controversial Urbach tailing universality, Eur. Phys. J. Plus 126 (2011) 1–4, https://doi.org/10.1140/epjp/i2011-11010-4.